Directional Persistence of Cell Migration Coincides with Stability of Asymmetric Intracellular Signaling

Michael C. Weiger, Shoeb Ahmed, Erik S. Welf, and Jason M. Haugh*
Department of Chemical and Biomolecular Engineering, North Carolina State University, Raleigh, North Carolina

ABSTRACT It has long been appreciated that spatiotemporal dynamics of cell migration are under the control of intracellular signaling pathways, which are mediated by adhesion receptors and other transducers of extracellular cues. Further, there is ample evidence that aspects of cell migration are stochastic: how else could it exhibit directional persistence over timescales much longer than typical signal transduction processes, punctuated by abrupt changes in direction? Yet the mechanisms by which signaling processes affect those behaviors remain unclear. We have developed analytical methods for relating parallel live-cell microscopy measurements of cell migration dynamics to the intracellular signaling processes that govern them. In this analysis of phosphoinositide 3-kinase signaling in randomly migrating fibroblasts, we observe that hot spots of intense signaling coincide with localized cell protrusion and endure with characteristic lifetimes that correspond to those of cell migration persistence. We further show that distant hot spots are dynamically and stochastically coupled. These results are indicative of a mechanism by which changes in a cell's direction of migration are determined by a fragile balance of relatively rapid intracellular signaling processes.

INTRODUCTION

The movement of eukaryotic cells on a uniformly adhesive surface is traditionally characterized as a persistent random walk. In this conceptual model, cells migrate along a fairly straight path during short time intervals, whereas over longer time intervals, the cells execute random changes in direction. The transition between these regimes occurs on a timescale of ~3–30 min, depending on the experimental context (1–4). Although it is clear that migration on a rigid surface coated with extracellular matrix (ECM) is rather different from cell motility in vivo, as seen in wound healing, tissue morphogenesis, and cancer metastasis (5–7), cell migration in two dimensions remains a viable system for studying fundamental aspects of cell migration. In particular, there is a gap in our understanding of how the various intracellular signal transduction pathways that regulate cell protrusion, adhesion, and contractility associated with cell migration are dynamically coordinated (8–10).

A diverse array of signaling enzymes and adaptor proteins have been implicated in random and spatially biased cell migration (11), and the importance of any one molecular pathway is likely to be context-dependent, even for the same cell. With that said, activation of phosphoinositide 3-kinase (PI3K)-dependent pathways apparently plays the most ubiquitous role, serving as a point of convergence for soluble and ECM-associated cues and a hub for signaling through Rho-family GTPases, serine-threonine kinases, and other modulators of adhesion and cytoskeletal dynamics (12). PI3Ks are lipid kinases that activate signaling by generating 3′-phosphorylated phosphoinositide (3′ PI) lipids, and accumulation of 3′ PIs at the plasma membrane can be monitored in living cells using certain fluorescent fusion protein biosensors (13). PI3K signaling has been implicated in numerous aspects of cell migration, including spatial gradient sensing, cell polarization, and modulation of cell protrusion, and perhaps this is why its precise mechanisms and roles in different cellular and environmental contexts have been difficult to parse (14–17). What is apparent, however, is that PI3K activation is among the furthest-upstream processes to exhibit symmetry breaking; in response to spatially uniform stimulation with chemoattractants, human leukocytes (differentiated HL-60 cells), vegetative *Dictyostelium discoideum* cells, and mouse fibroblasts all exhibit localized regions of 3′ PI enrichment, seen as patches or ''hot spots'' of higher biosensor fluorescence (16,18–20).

Recently, we used total internal reflection fluorescence (TIRF) microscopy to show that hot spots of PI3K signaling are also present in fibroblasts randomly migrating on immobilized fibronectin, and further, that the hot spots are dynamic and preferentially localized in membrane protrusions oriented in the direction of overall cell movement (17). Those observations have led us to ask how the spatial pattern of intracellular signaling, through PI3K and other pathways, might be related to the direction and efficiency of cell movement observed using live-cell fluorescence microscopy, and how the dynamics of hot spots and other important features of the signaling pattern might be related to local changes in cell motility. To address these questions, we have developed a collection of image analysis protocols that we call signaling vector analysis (SVA). After outlining the development of the approach, and its variations, we report its application to an expanded set of 28 randomly migrating fibroblasts; in these cells, nearly 1400 hot spots of PI3K signaling were identified, tracked, and related to

Submitted June 27, 2009, and accepted for publication September 25, 2009.

*Correspondence: jason_haugh@ncsu.edu

Editor: Denis Wirtz.

0006-3495/10/01/0067/9 $2.00

doi: 10.1016/j.bpj.2009.09.051

the morphodynamics of the cells as they moved. From these observations and analyses, we offer what to our knowledge is a new conceptual model of random migration persistence based on the protrusion of stochastically activated, yet coordinated, lamellipodia, reminiscent of a tug of war. By identifying the characteristic timescales associated with hot-spot dynamics, this conceptual model gives way to a quantitative one, in which signaling hot spots are maintained for an uncertain duration through a dynamic yet fragile equilibrium of relatively fast activation and deactivation processes.

MATERIALS AND METHODS

Cell culture and reagents

Stable expression of the 3′ phosphoinositide-specific biosensor construct EGFP-AktPH in NIH 3T3 mouse fibroblasts (American Type Culture Collection, Rockville, MD) was achieved by retroviral infection and puromycin selection, as previously described (17). The cells were subcultured using Dulbecco's modified Eagle's medium supplemented with 10% v/v fetal bovine serum and 1% v/v penicillin/streptomycin/glutamate as the growth medium. All tissue culture reagents were purchased from Invitrogen (Carlsbad, CA). Human plasma fibronectin was obtained from BD Biosciences (San Jose, CA) and Invitrogen.

Cell migration experiments

Glass coverslips were cleaned, sterilized, coated with fibronectin (10 μg/ml) for 1 h at 37°C, washed with deionized, sterile water, and dried within 30 min of the experiment. EGFP-AktPH-expressing cells were serum-starved for 2.5 h and then detached with a brief trypsin-EDTA treatment and suspended in the imaging buffer (20 mM HEPES, pH 7.4, 125 mM NaCl, 5 mM KCl, 1.5 mM $MgCl_2$, 1.5 mM $CaCl_2$, 10 mM glucose, 1% v/v fetal bovine serum, 2 mg/ml fatty-acid-free bovine serum albumin). After centrifugation at 100 $\times$ g for 3 min, the cells were resuspended in imaging buffer and plated on the fibronectin-coated coverslips at a density of 10,000 cells/ml and allowed to spread for 1 h before imaging. Mineral oil was layered on top of the buffer to prevent evaporation during the experiment.

TIRF microscopy

TIRF microscopy is used to selectively excite fluorophores within ~100 nm of the substratum-buffer interface, illuminating the plasma membrane contact area and, in fibroblasts, ~5–10% of the cytoplasm directly above it (21). Our prism-based TIRF microscope has been described in detail previously (22). EGFP was excited using a 60-mW 488-nm line from a tunable-wavelength argon ion laser head (Melles Griot, Irvine, CA). A 20× water immersion objective (Achroplan, 0.5 NA; Zeiss, Oberkochen, Germany) and 0.63× camera mount were used. Digital images, with 2 $\times$ 2 binning, were acquired at 2-min intervals using a Hamamatsu ORCA ER cooled CCD (Hamamatsu, Bridgewater, NJ), with a fixed exposure time $\times$ gain of 1000–1200 ms, and Metamorph software (Universal Imaging, West Chester, PA).

Image segmentation and implementation of macroscopic SVA

Image segmentation was performed as follows. A custom code was written in MATLAB (The MathWorks, Natick, MA) to read the image files as data matrices and process them using the k-means clustering method, which bins pixels by relative intensity, assuming a specified number (k) of peaks in the intensity distribution. For our images, $k = 4$ was found to be optimum. The pixels in the acellular background (lowest intensity) are grouped in bin 1, whereas regions of intense fluorescence (hot spots) are found in bin 4. For each cell, masks were generated that define regions of interest corresponding to the entire cell contact area (bins 2–4) and hot-spot regions (bin 4 only). MATLAB Image Processing Toolbox was used to determine the area (A), average intensity (F), and centroid coordinates of each labeled region, and a minimum area cutoff of 20 pixels was imposed on the hot spots to ensure that they are contiguous regions, not transient speckles.

For each cell image, the macroscopic signaling vector is calculated as follows (17) (Fig. 1 *a*). The coordinates of the cell's centroid are subtracted from those of each of its hot spots, i, defining the position of the hot spot relative to the cell centroid, $\mathbf{x}_i = (x_i,y_i)$, and its vector, $\mathbf{s}_i$, is defined with magnitude equal to the fluorescence volume (A_iF_i); the overall, resultant signaling vector $\mathbf{S}_\mathrm{R}$ is the sum of $\mathbf{s}_i$:

$$\mathbf{s}_i = A_iF_i\frac{\mathbf{x}_i}{\sqrt{x_i^2 + y_i^2}}; \quad \mathbf{S}_\mathrm{R} = \sum_{i=1}^{N}\mathbf{s}_i. \tag{1}$$

The temporal resolution of image acquisition, Δt (2 min), was found to be too fine for tracking the cell (centroid) movement vector, defined as $\mathbf{C}$; a time step of $6\Delta t$ (12 min) was found to be optimal. For the purpose of vector correlation, the signaling vector assigned to a particular cell movement step, from t_i to $t_i + 6\Delta t$, was taken as the average of the six $\mathbf{S}_\mathrm{R}$ calculated for t_i, $t_i + \Delta t$, …, $t_\mathrm{i} + 5\Delta t$ ($\mathbf{S}_\mathrm{Ave}$).

A method for correlating any two sets of vectors was implemented in MATLAB, using a correlation coefficient metric, ρ, defined in detail by Hanson et al. (23). The metric incorporates both the magnitudes and directions of the two vector sets and ranges from -1 (perfectly anticorrelated) to 1 (perfectly correlated); $\rho = 0$ indicates completely uncorrelated data. The method was applied to $\mathbf{S}_\mathrm{Ave}$ and $\mathbf{C}$, with varied time lag (positive time lag indicating that the signaling vector preceded the cell movement), and the same procedure was used to autocorrelate each of the vectors.

Hot-spot tracking for microscopic SVA

Hot-spot regions, identified as described in the previous section, were tracked using custom MATLAB codes as follows. For each hot-spot region in a particular image, the algorithm looks for one or more region(s) with overlapping pixels in the next two frames (thus guarding against the possibility that the hot spot was missed for a frame). If there are none, it is marked as a death event for the hot spot in the previous image. Conversely, if the same procedure is performed in reverse, and it is found that a hot spot in the next image does not overlap with any in the previous frame, it is marked as a birth event. If a hot spot is found to overlap with only one hot spot in the next frame (or with one hot spot two frames later, if the hot spot was missed for a frame, as outlined above), the movement is assigned to the same hot-spot path. If, on the other hand, a hot spot in the previous image is found to overlap with two or more hot spots in the next image, it is counted as a branching event; the same outcome when the procedure is performed in reverse is counted as a merging event. A branching event is disregarded if the hot spot apparently splits and then merges within the next two frames (in which case the merging event is also disregarded). This added step guards against the possibility that the algorithm temporarily misses the continuity of a weaker, but nonetheless intact, hot spot. Another potential artifact is the possibility that a hot spot moves so quickly during a 2-min interval that it causes a break in the path of continuous overlap, resulting in an apparent death of a hot spot and birth of another in the same interval. In the 28 cells analyzed, there were 247 instances of coincident death-birth, and these were checked manually for interruption of tracking; none were obvious failures of the tracking algorithm, but in nine cases (3.6%), the death and birth events were such that the determination was ambiguous.

The path of each hot-spot region determines its lifetime and net distance moved (the distance between its centroid positions at birth and death). All combinations of branched and merged hot-spot paths were considered. For example, consider a hot spot that is born and later merges with another hot spot that had not previously branched or merged; these two hot-spot paths would be considered distinct paths that now share a common subpath.

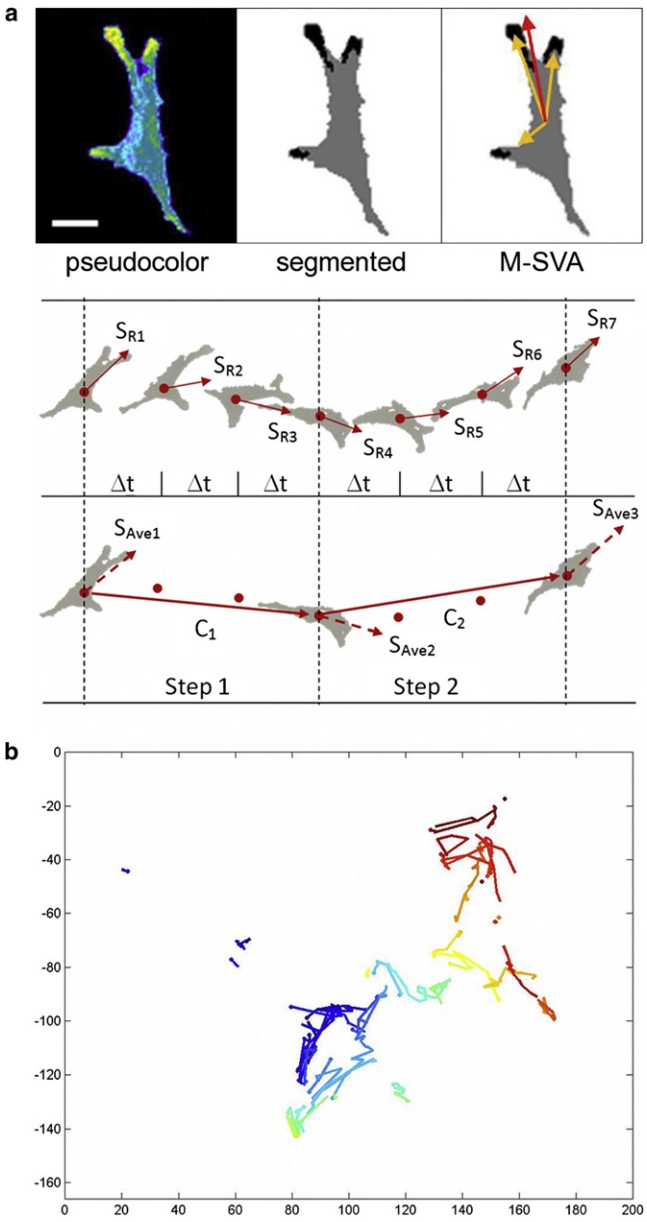

FIGURE 1 Illustration of SVA. (*a*) Constructing the macroscopic signaling vector for M-SVA. (*Upper*) A representative TIRF image of a GFP-AktPH-expressing fibroblast's contact area is shown in pseudocolor (*left*) and after segmentation (*middle*) using the *k*-means algorithm ($k = 4$). Pixels in the highest intensity bin (hot spots) are shown in black, and other pixels assigned to the cell (bins 2 and 3) are shown in gray. Construction of the resultant macroscopic signaling vector is shown at right. Scale bar, 20 μm. (*Lower*) A cartoon illustrates our scheme for averaging signaling vectors ($\mathbf{S}_R$) over time periods appropriate for tracking cell migration ($\mathbf{C}$); it is noted that the time interval for cell tracking was $6\Delta t = 12$ min, not $3\Delta t$ as shown (see Materials and Methods). (*b*) Tracking hot-spot dynamics and fates (μ-SVA). The plot shown indicates the (x,y) positions of each fluorescent hot-spot centroid from birth to death, accounting also for hot-spot branching and merging events, for a representative cell (see also Fig. 2, *a* and *b*). Each hot spot's path is connected by lines, color-coded from cool to warm according to advancing time (time interval, 2 min). This sequence is animated, alongside a pseudocolor TIRF movie of the migrating cell, in Movie S2.

If at some point the merged hot spot were to branch into three hot spots, then in this example there would be six distinct hot-spot paths from that point forward.

Simple stochastic model of intracellular signaling dynamics

A compartmental, stochastic model is posed for the purpose of exploring the potential basis for coupled dynamics of competing hot-spot regions. There are two species in the model, a trigger and an integrator. The numbers of trigger and integrator molecules in compartment j, T_j and I_j, respectively, evolve according to

$$\frac{dT_j}{dt} = k_1(1 + \alpha I_j)T_{\text{free}} - k_{-1}T_j; \tag{2}$$

$$\frac{dI_j}{dt} = k_2 T_j - k_{-2} I_j, \tag{3}$$

where T_{free} is the number of free, rapidly diffusible trigger molecules; k_1, k_{-1}, k_2, and k_{-2} are rate constants; and α is a constant positive feedback parameter. The total number of trigger molecules, defined as T_0, is assumed to be constant, so that

$$T_{\text{free}} = T_0 - \sum_j T_j. \tag{4}$$

The depletion of free trigger molecules is what couples the dynamics of the compartments, whereas the local positive feedback reinforcing incorporation of free trigger tends to amplify the stochastic fluctuations. Mathematically, this model is similar to the "one-component" mechanism of chemotactic gradient sensing proposed by Postma and van Haastert (24).

The forward and reverse reactions in Eqs. 2 and 3 were modeled as discrete probabilistic transitions, and stochastic simulations were implemented using the standard Next Reaction Method (25), coded in MATLAB. For the model results (see Fig. 6 *b*), the number of subcompartments was 5, and the parameter values were $k_1 = 2$ min^{-1}, $k_{-1} = 3$ min^{-1}, $\alpha = 10$, $T_0 = 10$, $k_2 = 10$ min^{-1}, and $k_{-2} = 1$ min^{-1}. Under these conditions, the integrator tends to be amplified relative to the trigger by a factor of $k_2/k_{-2} = 10$; this number is arbitrary as long as it is sufficiently large and the value of α is scaled accordingly.

RESULTS

Development of SVA

The macroscopic signaling vector is constructed as described under Materials and Methods (Fig. 1 *a*). It is a fluorescence-weighted average of the orientations of PI3K signaling hot spots relative to the centroid of each cell's contact area (visualized by TIRF microscopy), and its magnitude reflects the sizes, intensities, and spatial asymmetry of the hot spots, determined from a single, static image. Hot spots are identified using standard image segmentation. Thus, to the extent that the localization of PI3K signaling is associated with cell motility, the signaling vector offers a prediction of the direction and/or speed of net cell movement, and changes in the signaling vector with time should determine or correspond with changes in cell migration behavior. The conceptual model, consistent with observations of the cells (Movie S1 in the Supporting Material), is that hot spots of PI3K signaling engage in a "tug-of-war", vying to determine

the direction of cell movement; it is further posited that the relative amount of fluorescence in each hot spot determines its influence on translocation of the cell centroid. We refer to this proposed relationship between signaling pattern and overall cell movement as macroscopic SVA (M-SVA).

We are also interested in the dynamics and fates of the individual hot spots (Fig. 1 *b* and Movie S2). If one were to track the motions of hot spots, would their lifetimes or velocities depend on their relative fluorescence levels? We also seek to characterize the rates of stochastic birth and death of individual hot spots and to determine whether or not such events are coupled. For instance, if the amount of PI3K or another key molecular component were stoichiometrically limiting, one might expect that the death of one hot spot would be followed by the birth of another (or vice versa) with a greater than average probability. We refer to the tracking of individual hot-spot movements and fates as microscopic SVA (μ-SVA).

Net cell movement during random fibroblast migration is spatiotemporally correlated with the intracellular pattern of PI3K signaling

We first demonstrate that the macroscopic signaling vector is generally aligned with overall cell migration, extending our previous analysis (17) (Fig. 2). Using TIRF microscopy, we monitored the PI3K signaling pattern and contact area centroid movement of 28 NIH 3T3 cells as they migrated on fibronectin. As shown qualitatively for a representative cell in Fig. 2, *a* and *b*, the centroid migration vector typically follows the asymmetry of 3′ PI localization, as indicated by the calculated signaling vector. This cell is the same as that depicted in Fig. 1 *b* and Movie S2; TIRF movies of four other migrating cells are shown in Movie S1 for comparison. For each cell, we quantified the alignment of the two vectors using a correlation coefficient metric that accounts for vector magnitudes and directions (23) and compared signaling and cell movement vectors with varying time lag (Fig. 2 *c*). Within the temporal resolution of our analysis, the highest mean correlation was found at zero time lag, when the majority of the cells exhibited positive correlation coefficient values >0.5 (Fig. 2 *d*). We also explored alternative definitions of the signaling vector, with hot spots weighted differently (Fig. S1). As expected, the correlation was relatively poor when the signaling vector did not account for the relative sizes or intensities of the PI3K hot spots.

The breadth of the peak in Fig. 2 *c*, exhibiting positive mean correlation coefficients for time shifts within ~20 min in either direction, is attributed to the similar persistence of PI3K signaling and cell movement. Indeed, the correlation coefficient for each vector with itself (averaged over the 28 cells) exhibits an exponential dependence on time lag, as anticipated, and the associated time constants for the signaling vector (18.3 min) and cell velocity vector (13.6 min) are comparable (Fig. 2, *e* and *f*). Taken together,

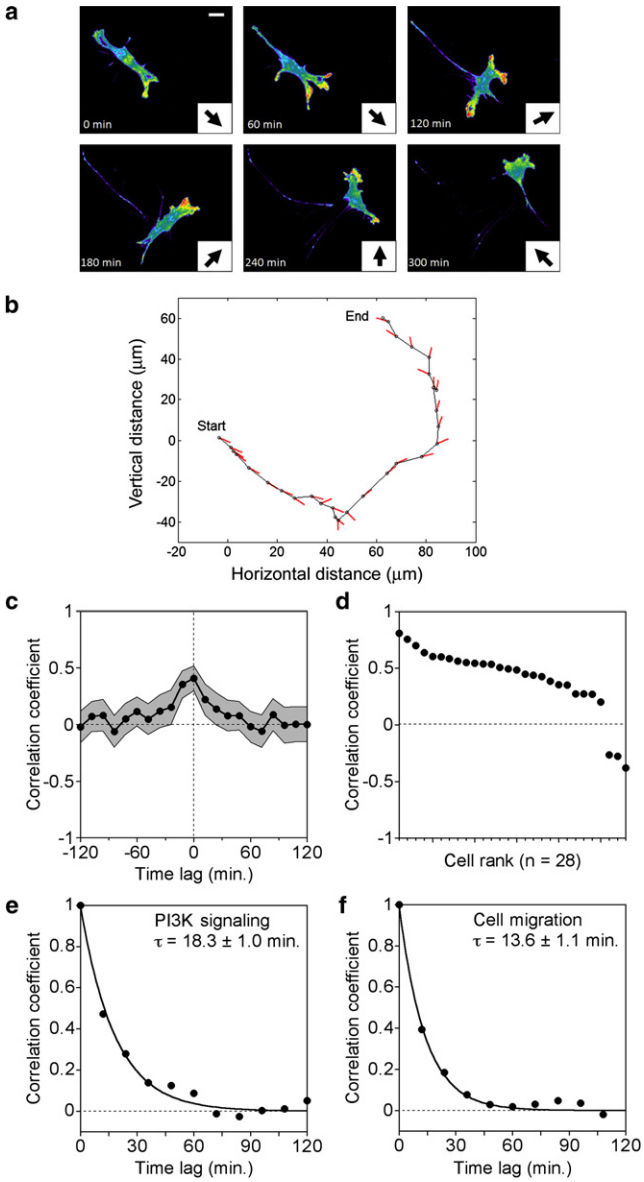

FIGURE 2 Macroscopic PI3K signaling vector as a predictor of cell movement. (*a*) TIRF montage depicting signaling and migration vectors during random migration; the time relative to the start of image acquisition is indicated. Scale bar, 20 μm. (*b*) Migration path of the centroid for the cell shown in *a*, measured at 12-min intervals (*circles*). The direction of the signaling vector is indicated by a short line emanating from each centroid point. (*c*) Correlation of PI3K signaling and centroid velocity vectors. The time lag is the interval between measurements of signaling and migration vectors, and the correlation coefficient means (*circles*) and 95% confidence intervals (*gray regions*) are shown for $n = 28$ cells. (*d*) Correlation coefficients for individual cells at zero time lag, ranked in descending order. (*e* and *f*) The persistence of cell movement is consistent with that of the macroscopic PI3K signaling vector. The two vector quantities were autocorrelated, and the resulting correlation coefficients were averaged for the 28 cells and fit to an exponential distribution, $\exp(-t/\tau)$, where t is the time lag and τ is the apparent time constant of change.

these results indicate that changes in cell migration behavior occur in tandem with changes in the pattern of PI3K signaling.

Hot spots of PI3K signaling are enriched in regions of membrane protrusion

According to our conceptual model, local PI3K signaling dynamics are related to asymmetric membrane protrusion. If so, another quantitative way to test the model is to demonstrate that PI3K hot spots are enriched in the protruded area (PA), determined for each cell and for a certain time interval (12 min, consistent with the analysis in Fig. 2), and much less so in the corresponding retracted area (RA) (Fig. 3 *a*). To show this, we define the level of enrichment, E, as the fraction of the PA or RA populated with hot-spot pixels divided by the fraction of the total contact area (in the earlier image) populated with hot-spot pixels; $E > 1$ means that hot spots are enriched in the region of interest. The time-averaged means for the 28 cells in our cohort range from 0.91–6.3 for the PA (3.0 ± 1.5, mean ± SD) and from 0.07–1.3 for the RA (0.61 ± 0.37, mean ± SD). The plot in Fig. 3 *b* shows that all 28 cells have significantly higher enrichment in the PA ($p = 5 \times 10^{-11}$, paired t-test).

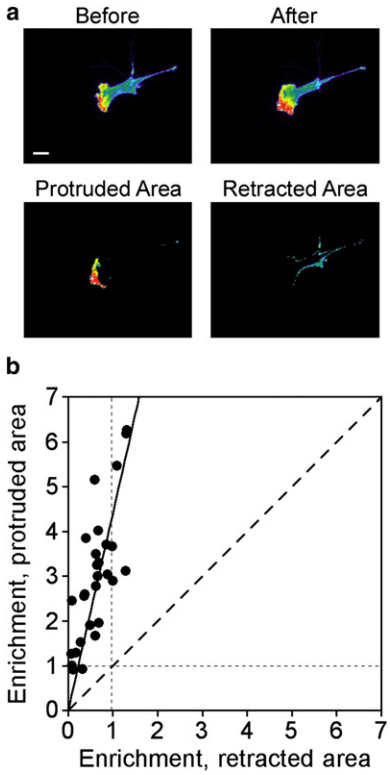

FIGURE 3 PI3K signaling hot spots tend to be localized in regions of membrane protrusion. (*a*) TIRF images, separated by 12-min intervals, are compared so as to determine the protruded and retracted areas. Pixels in the protruded area are associated with the cell contact area in the more recent image but were in the background in the earlier image; conversely, pixels in the retracted area were in the contact area in the earlier image but are in the background in the more recent image. Scale bar, 20 μm. (*b*) The enrichment, E, of a region is defined as the fraction of its pixels belonging to hot spots, compared to that of the whole-cell contact area. Circles indicate the time-averaged mean values of E in the protruded and retracted areas for each of 28 cells (see main text for further description). An E value >1 indicates that the region of interest has, on average, a higher percentage of hot-spot pixels than the entire contact area.

Hot spots with greater PI3K signaling activity tend to be more stable and therefore move more productively

Having characterized the spatial asymmetry and temporal persistence of the overall PI3K signaling pattern and its relation to net cell protrusion and movement, we employed μ-SVA to track the dynamics of individual hot spots (their 3′ PI accumulation kinetics and movements). This allowed us to address the more fundamental question of how local membrane protrusion depends on the level of PI3K signaling (Fig. 4). The time-averaged fluorescence volume (A_iF_i), normalized by the fluorescence volume of the cell contact area (averaged over the same time period), was calculated for each of 1395 hot-spot paths, and hot-spot paths were binned into three equal-sized groups ($n = 465$) based on this metric of PI3K signaling (Fig. 4 *b*, *Low*, *Intermed.*, and *High*).

The hot-spot paths with higher relative PI3K signaling levels tend to move more productively, as measured by the distance between birth and death points (Fig. 4 *c*). The mean distances of the three bins are 8, 22, and 30 μm,

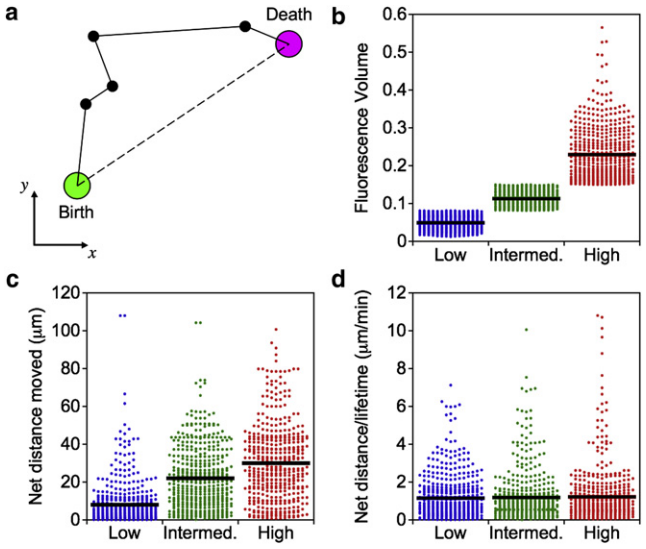

FIGURE 4 Productive movements of individual hot spots depend on their PI3K signaling levels. (*a*) Hot-spot paths were tracked from birth to death using μ-SVA. The schematic illustrates the determination of the net distance traveled (*dashed line*) and lifetime (number of segments in the path, converted to minutes). (*b–d*) The hot spots were binned into three, equal-sized groups ($n = 465$) based on their normalized, time-averaged fluorescence volume (see the main text for details) (*b*), from which was determined their net distance traveled from birth to death (*c*) and their net distance traveled divided by lifetime (*d*). Each hot-spot path is represented by a dot, and the black bars indicate mean values.

respectively, and all pairwise comparisons among these groups are statistically significant ($p < 10^{-10}$, Student's *t*-test). A similar trend was found when comparing the lifetimes of the three groups (results not shown), and when the net movement of each hot-spot path is normalized by its lifetime, the three groups binned by fluorescence level are not statistically different (Fig. 4 *d*; $p > 0.45$ for all comparisons by Student's *t*-test). This implies that hot spots with greater PI3K signaling move more productively because they live longer, not because they move more efficiently.

The persistence of cell migration is consistent with the characteristic lifetime of individual PI3K hot spots

The information gathered using the μ-SVA approach can also be used to quantify hot-spot fates, which we characterize in terms of birth (appearance of a new hot spot), death (disappearance of a hot spot), branching (splitting of one hot spot into two or more), and merging (coalescing of multiple hot spots into one) events. The rate of each of these processes was taken as the total number of events divided by the total time of observation. As noted under Materials and Methods, the disappearance of a hot spot in one frame followed by the appearance of an overlapping hot spot in the next frame was not considered a bona fide death (or birth) event, and a hot spot splitting and then coalescing within two successive frames (4 min) was not considered a bona fide branching (or merging) event. We found that these steps were effective in filtering out spurious fate assignments by the hot-spot tracking algorithm.

The average number of hot spots, N, and the frequencies of the four fate events are listed in Table 1. We find good agreement between the inverse of the specific death rate, N/V_{death} (18.7 min), and the time constant of macroscopic signaling vector persistence (18.3 min; Fig. 2 *e*). Because the rates of birth and death are closely matched ($V_{\text{birth}} \approx V_{\text{death}}$, and, because the number of hot spots is approximately conserved, $V_{\text{branch}} \approx V_{\text{merge}}$), the value of N/V_{birth} (19.8 min) also captures the timescale of major changes in the signaling pattern. Further, there is good correspondence between the timescale of overall hot-spot consumption (or generation), calculated as $N/(V_{\text{death}} + V_{\text{merge}})$ (13.4 min), and the time constant of cell movement persistence (13.6 min; Fig. 2 *f*).

TABLE 1 Parameters characterizing the fates of PI3K signaling hot spots

Parameter	Value (mean ± SD)
Number of hot spots, N	2.3 ± 0.7
Average birth rate, V_{birth}	0.117 ± 0.057 min^{-1}
Average death rate, V_{death}	0.123 ± 0.061 min^{-1}
Average branch rate, V_{branch}	0.054 ± 0.036 min^{-1}
Average merge rate, V_{merge}	0.049 ± 0.037 min^{-1}

The fates and dynamics of distinct PI3K hot spots are stochastically coupled

We next asked whether hot spot births and deaths are random or coupled events. To answer this question, we determined, for each cell, the waiting times between successive hot-spot births (birth-birth), successive deaths (death-death), death and birth events (death-birth, where each birth is matched with the most recent death), and likewise birth and death events (birth-death). If the second of the two events were random, the waiting-time distribution would not depend on the nature of the first; otherwise, the two events may be considered coupled.

As shown in Fig. 5, *a* and *b*, the aggregate waiting time distributions pooled from all 28 cells exhibit a degree of positive, nonrandom coupling between birth and death events, characterized by sharper peaks at ~2–6 min and lower mean waiting times (~5.8 min for death-birth and 5.7 min for birth-death) in comparison with those of birth-birth (8.0 min) and death-death (7.9 min). Fig. 5, *c* and *d*, shows that this positive coupling is prevalent when comparing mean waiting times for individual cells; mean death-birth and birth-death waiting times tend to be significantly shorter than the mean birth-birth and death-death waiting times, respectively ($p = 9 \times 10^{-6}$ and 2×10^{-4}, paired *t*-tests). We conclude that the birth of a new hot spot makes existing

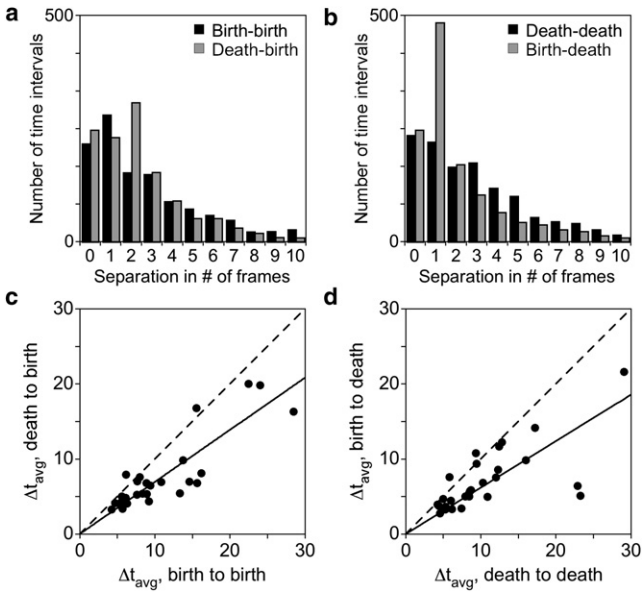

FIGURE 5 Hot-spot birth and death events are positively coupled. Individual PI3K signaling hot spots were tracked using μ-SVA, and waiting-time distributions were determined for intervals between births, between deaths, and between death-birth and birth-death events. (*a*) Aggregate (pooled data for 28 cells) distributions of birth-birth and death-birth waiting times. (*b*) Aggregate distributions of death-death and birth-death waiting times. (*c*) Scatter plot showing the mean birth-birth and death-birth waiting times (in minutes) for each cell. (*d*) Scatter plot showing the mean death-death and birth-death waiting times (in minutes) for each cell.

hot spots more vulnerable to dying out and, conversely, the death of a hot spot tends to hasten the birth of another.

Another way to illustrate this coupling is to examine the kinetics of each hot spot's fluorescence volume (A_iF_i), normalized by that of the whole cell, in relation to those of other hot spots. As shown in Fig. 6 *a*, for a representative cell, the fluorescence of each hot spot exhibits a great deal of volatility; the apparent fluctuations reflect changes in fluorescence intensity as well as region size, as seen clearly for the migrating cells shown in Movie S1 and Movie S2. Consistent with the analysis shown in Fig. 5, Fig. 6 *a* shows that births of new hot spots tend to precipitate deaths of other hot spots and vice versa, and the fluctuations of each hot spot's fluorescence tend to be negatively correlated with those of others present at the same time (Fig. 6 *a*, *inset*). The representative cell also exhibits the tendency of these ''seesaw'' dynamics to occur in rapid succession, relative to the temporal resolution of our image acquisition.

The coupling of PI3K hot spot birth/death fates and fluorescence dynamics in distant regions of the cell suggests a hypothetical mechanism wherein hot spots are triggered by a component that is recruited from a common, cytosolic pool. To test the plausibility of this hypothesis, we formulated a basic computational model in which the recruitment of the trigger component is stabilized through positive feedback, and we evaluated the characteristics of the model by stochastic simulation (Materials and Methods). As shown in Fig. 6 *b*, the positive feedback mechanism imposes a sensitivity of each hot spot's dynamics to those of others, consistent with the experimental observations presented in Fig. 6 *a*, and the model recapitulates the finding that more intense hot spots tend to be more stable. The average number of hot spots above threshold and their average lifetime are tunable, depending on the specified values of the model parameters (results not shown), and the parameter values chosen appear to reproduce the typical hot-spot lifetime of ~15–20 min.

DISCUSSION

Models of intracellular signal transduction (26,27) and of cell motility (28), both conceptual and mathematical, are now commonplace; however, except perhaps in the context of amoeboid chemotaxis (29), these two phenomena are generally considered separately. We see two reasons for this. First, relating intracellular signaling dynamics to the cell responses they govern requires long-term monitoring of both processes. This is now possible using fluorescent signaling biosensors and spatiotemporally resolved live-cell imaging. Second, the intracellular signaling pattern and cell migration are quantified in different terms: fluorescence contained within the cellular boundary and movements of the boundary, respectively. Therefore, it is not immediately clear how one would relate the two measurements. The analyses developed here, M-SVA and μ-SVA, address this need and are meant to complement other

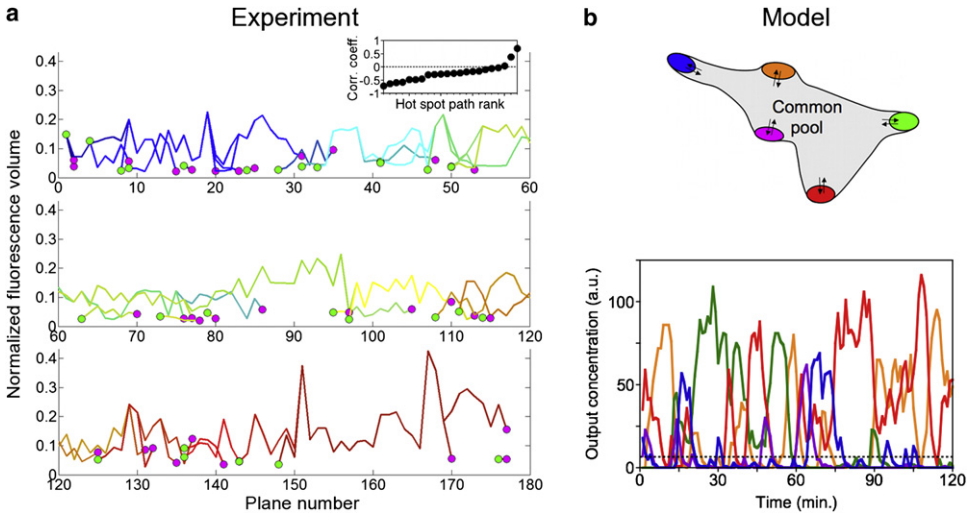

FIGURE 6 Stochasticity of PI3K signaling during random cell migration. (*a*) Hot-spot fluorescence kinetics exhibit dynamic, counteracting fluctuations. A representative cell was analyzed using μ-SVA, and the normalized fluorescence volume of each of its hot spots ($A_iF_i/A_{cell}F_{cell}$) is plotted as a function of time (in number of image planes, time interval = 2 min). The dynamics of each hot spot is assigned a unique color based on when it appeared, and the circle symbols indicate the recorded birth and death events. (*Inset*) Ranked plot of correlation coefficients (mean = −0.23, n = 22), where the normalized fluorescence volume of each unique hot-spot subpath was correlated against the sum of all others present at the same time; time intervals during which there was only one hot-spot subpath (i.e., when no others were present) were discarded from the analysis, and only those subpaths with five or more values to correlate were included. (*b*) Simple model of signaling pattern fragility. A stochastic model (Materials and Methods) was implemented using the Next Reaction Method, and the concentration of the integrator, I_j, is plotted as a function of time for each of five regions (subcompartments). The excitability of the model is caused by competition for a limiting component and positive feedback. The dotted, horizontal line on the plot illustrates that there is a level below which the signal could not be distinguished from noise.

computational approaches for analyzing fluorescence microscopy data in cell biology (30–32). The approach is based on the concept that hot-spot regions of intense signaling promote local membrane protrusion, effectively pushing the cell in different directions.

The SVA approach was applied to PI3K signaling in randomly migrating fibroblasts, and tracking the dynamics and fates of PI3K hot spots led us to develop a phenomenological model of cell migration. In this model, the stability of each hot spot, stochastically coupled to the dynamics of other hot spots, determines the persistence of cell movement. The timescale of hot-spot turnover was 15–20 min for the experimental conditions used here, which is much slower than the underlying dynamics of intracellular signaling; we know that the mean lifetime of 3′ PI lipids is only ~1 min in these cells (21), for example. Therefore, hot-spot fates must be governed by comparatively rare stochastic transitions that, through a coupling mechanism, have the potential to dramatically perturb, and thus remodel, the pattern of intracellular signaling.

We found that a simple model in which different regions of the cell compete for a limiting component, subject to positive feedback, reproduces several aspects of the observed signaling dynamics that are, in turn, correlated with cell protrusion and movement. The interpretation is that signaling hot spots arise and are maintained through a dynamic—and ultimately fragile—equilibrium of relatively fast molecular recruitment processes. An important aspect of the hypothetical model is positive feedback, which could be chemical (24) or mechanical (33) in nature and which might be influenced by changes in cell morphology (34,35) during migration; indeed, we were not able to definitively resolve from our data whether changes in PI3K signaling precede changes in cell motility or vice versa. If conceptualized as a biochemical feedback, wherein the product of an enzymatic reaction contributes to enhanced recruitment of the enzyme, our model is similar to the ''one-component'' mechanism of chemotactic gradient sensing proposed by Postma and van Haastert (24). Also in the realm of chemotaxis, more biochemically explicit models invoking positive feedback between PI3K and Rho- and Ras-family GTPases have been formulated more recently (36–38). A key distinction in the model presented here is its focus on stochastic rather than deterministic processes. Obviously, in the absence of a spatial cue, the deterministic version of the model can only generate a homogeneous pattern.

Whereas our simple model is based on depletion of a limiting component from the cytosol, another well-known (and mathematically similar) coupling mechanism is the activation of a fast-diffusing (i.e., global) inhibitor (29,39). The influence of an inhibitor could result in larger, even catastrophic fluctuations if it were to act infrequently to slow down or halt the incorporation of signaling components into hot-spot regions, as conceptualized recently for the effect of capping protein on actin filament dynamics in filopodia (40).

The analyses reported here rely on SVA methods that should be portable to other systems, provided that the boundaries of the cell and its local regions of higher fluorescence intensity are clearly distinguishable. Excellent resolution was achieved in our experiments through the use of TIRF microscopy, so it remains to be seen how well the approach would work using other microscopy modes, or, with certain modifications, for migration in three dimensions (where TIRF is not possible). For measurements in which only a slice of the cell cortex is resolved, using confocal fluorescence microscopy, for example, other image analysis methods might be more useful on the front end (30). Nevertheless, it is envisioned that SVA could serve as a tool for unraveling the spatial regulation of cell motility at the molecular level, regardless of context.

SUPPORTING MATERIAL

Two movies and a figure are available at http://www.biophysj.org/biophysj/supplemental/S0006-3495(09)01565-3.

This work was supported by the National Science Foundation through the Science and Technology Center Program (CHE-9876674) and grant CBET-0828936. Mathematical modeling work was partially supported by the Cell Migration Consortium under National Institutes of Health grant U54-GM064346.

REFERENCES

1. Berg, H. C. 1983. Random Walks in Biology. Princeton University Press, Princeton, N.J.
2. Dunn, G. A., and A. F. Brown. 1987. A unified approach to analysing cell motility. *J. Cell Sci.* 8 (Suppl.):81–102.
3. Lauffenburger, D. A., and J. L. Linderman. 1993. Receptors: Models for Binding, Trafficking, and Signaling. Oxford University Press, New York.
4. Dickinson, R. B., and R. T. Tranquillo. 1993. Optimal estimation of cell-movement indexes from the statistical analysis of cell tracking data. *AIChE J.* 39:1995–2010.
5. Green, J. A., and K. M. Yamada. 2007. Three-dimensional microenvironments modulate fibroblast signaling responses. *Adv. Drug Deliv. Rev.* 59:1293–1298.
6. Prasad, M., and D. J. Montell. 2007. Cellular and molecular mechanisms of border cell migration analyzed using time-lapse live-cell imaging. *Dev. Cell.* 12:997–1005.
7. Condeelis, J., and J. E. Segall. 2003. Intravital imaging of cell movement in tumours. *Nat. Rev. Cancer.* 3:921–930.
8. Maheshwari, G., and D. A. Lauffenburger. 1998. Deconstructing (and reconstructing) cell migration. *Microsc. Res. Tech.* 43:358–368.
9. Ridley, A. J., M. A. Schwartz, …, A. R. Horwitz. 2003. Cell migration: integrating signals from front to back. *Science.* 302:1704–1709.
10. Sabouri-Ghomi, M., Y. Wu, …, G. Danuser. 2008. Visualizing and quantifying adhesive signals. *Curr. Opin. Cell Biol.* 20:541–550.
11. Wang, Y., S. J. Ding, …, R. L. Klemke. 2007. Profiling signaling polarity in chemotactic cells. *Proc. Natl. Acad. Sci. USA.* 104:8328–8333.
12. Cain, R. J., and A. J. Ridley. 2009. Phosphoinositide 3-kinases in cell migration. *Biol. Cell.* 101:13–29.
13. Várnai, P., and T. Balla. 2006. Live cell imaging of phosphoinositide dynamics with fluorescent protein domains. *Biochim. Biophys. Acta.* 1761:957–967.

14. Loovers, H. M., M. Postma, …, P. J. van Haastert. 2006. Distinct roles of PI(3,4,5)P3 during chemoattractant signaling in *Dictyostelium*: a quantitative in vivo analysis by inhibition of PI3-kinase. *Mol. Biol. Cell.* 17:1503–1513.

15. Hoeller, O., and R. R. Kay. 2007. Chemotaxis in the absence of PIP3 gradients. *Curr. Biol.* 17:813–817.

16. Sasaki, A. T., C. Janetopoulos, …, R. A. Firtel. 2007. G protein-independent Ras/PI3K/F-actin circuit regulates basic cell motility. *J. Cell Biol.* 178:185–191.

17. Weiger, M. C., C.-C. Wang, …, J. M. Haugh. 2009. Spontaneous phosphoinositide 3-kinase signaling dynamics drive fibroblast spreading and random migration. *J. Cell Sci.* 122:313–323.

18. Servant, G., O. D. Weiner, …, H. R. Bourne. 2000. Polarization of chemoattractant receptor signaling during neutrophil chemotaxis. *Science.* 287:1037–1040.

19. Postma, M., J. Roelofs, …, P. J. Van Haastert. 2003. Uniform cAMP stimulation of *Dictyostelium* cells induces localized patches of signal transduction and pseudopodia. *Mol. Biol. Cell.* 14:5019–5027.

20. Schneider, I. C., E. M. Parrish, and J. M. Haugh. 2005. Spatial analysis of 3′ phosphoinositide signaling in living fibroblasts: III. influence of cell morphology and morphological polarity. *Biophys. J.* 89:1420–1430.

21. Schneider, I. C., and J. M. Haugh. 2004. Spatial analysis of 3′ phosphoinositide signaling in living fibroblasts: II. Parameter estimates for individual cells from experiments. *Biophys. J.* 86:599–608.

22. Schneider, I. C., and J. M. Haugh. 2005. Quantitative elucidation of a distinct spatial gradient-sensing mechanism in fibroblasts. *J. Cell Biol.* 171:883–892.

23. Hanson, B., K. Klink, …, C. J. Willmott. 1992. Vector correlation: review, exposition and geographic application. *Ann. Assoc. Am. Geogr.* 82:103–116.

24. Postma, M., and P. J. M. Van Haastert. 2001. A diffusion-translocation model for gradient sensing by chemotactic cells. *Biophys. J.* 81: 1314–1323.

25. Gibson, M. A., and J. Bruck. 2000. Efficient exact stochastic simulation of chemical systems with many species and many channels. *J. Phys. Chem. A.* 104:1876–1889.

26. Kholodenko, B. N. 2006. Cell-signalling dynamics in time and space. *Nat. Rev. Mol. Cell Biol.* 7:165–176.

27. Haugh, J. M. 2008. Mathematical modeling of biological signaling networks. *In* Wiley Encyclopedia of Chemical Biology. T. P. Begley, chief advisor, editor. John Wiley & Sons, New York.

28. Mogilner, A. 2009. Mathematics of cell motility: have we got its number? *J. Math. Biol.* 58:105–134.

29. Iglesias, P. A., and P. N. Devreotes. 2008. Navigating through models of chemotaxis. *Curr. Opin. Cell Biol.* 20:35–40.

30. Dormann, D., T. Libotte, …, T. Bretschneider. 2002. Simultaneous quantification of cell motility and protein-membrane-association using active contours. *Cell Motil. Cytoskeleton.* 52:221–230.

31. Machacek, M., and G. Danuser. 2006. Morphodynamic profiling of protrusion phenotypes. *Biophys. J.* 90:1439–1452.

32. Dorn, J. F., G. Danuser, and G. Yang. 2008. Computational processing and analysis of dynamic fluorescence image data. *Methods Cell Biol.* 85:497–538.

33. Novak, I. L., B. M. Slepchenko, …, L. M. Loew. 2004. Cooperativity between cell contractility and adhesion. *Phys. Rev. Lett.* 93:268109.

34. Meyers, J., J. Craig, and D. J. Odde. 2006. Potential for control of signaling pathways via cell size and shape. *Curr. Biol.* 16:1685–1693.

35. Haugh, J. M. 2007. Membrane-binding/modification model of signaling protein activation and analysis of its control by cell morphology. *Biophys. J.* 92:L93–L95.

36. Dawes, A. T., and L. Edelstein-Keshet. 2007. Phosphoinositides and Rho proteins spatially regulate actin polymerization to initiate and maintain directed movement in a one-dimensional model of a motile cell. *Biophys. J.* 92:744–768.

37. Onsum, M., and C. V. Rao. 2007. A mathematical model for neutrophil gradient sensing and polarization. *PLoS Comput. Biol.* 3:436–450.

38. Skupsky, R., W. Losert, and R. J. Nossal. 2005. Distinguishing modes of eukaryotic gradient sensing. *Biophys. J.* 89:2806–2823.

39. Meinhardt, H., and A. Gierer. 2000. Pattern formation by local self-activation and lateral inhibition. *Bioessays.* 22:753–760.

40. Zhuravlev, P. I., and G. A. Papoian. 2009. Molecular noise of capping protein binding induces macroscopic instability in filopodial dynamics. *Proc. Natl. Acad. Sci. USA.* 106:11570–11575.